Self DNA perpetuates IPF lung fibroblast senescence in a cGAS-dependent manner

Michael Schuliga[1,2], Jane Read[1,2], Kaj EC Blokland[1,2,3,4], David W Waters[1,2], Janette Burgess[3], Cecilia Prele[5,6,7], Steven E Mutsaers[5,6], Jade Jaffar[8], Glen Westall[8], Andrew Reid[2,9], Allen James[10], Christopher Grainge[2,9,10] and Darryl A Knight[1,2,11]

[1]School of Biomedical Sciences and Pharmacy, University of Newcastle, Callaghan, NSW, Australia; [2]Hunter Medical Research Institute, New Lambton Heights, NSW, Australia; [3]University of Groningen, University Medical Center Groningen, Department of Pathology and Medical Biology, Groningen Research Institute of Asthma and COPD and KOLFF Institute, Netherlands; [4]National Health and Medical Research Council Centre of Research Excellence in Pulmonary Fibrosis, Sydney, New South Wales, Australia; [5]Institute for Respiratory Health, University of Western Australia, Nedlands, WA, Australia; [6]Centre for Cell Therapy and Regenerative Medicine, School of Biomedical Sciences, University of Western Australia, Crawley, WA, Australia; [7]Ear Science Institute Australia, WA, Australia; [8]Allergy, Immunology and Respiratory Medicine, Alfred Hospital, Prahran, Victoria, Australia; [9]School of Medicine and Public Health, University of Newcastle, Callaghan, NSW, Australia; [10]John Hunter Hospital, Newcastle, NSW; [11]Providence Health Care Research Institute, Vancouver, British Columbia, Canada.

Correspondence Dr. Michael Schuliga, School of Biomedical Sciences and Pharmacy, University of Newcastle, HMRI Building, Callaghan, NSW 2308, Australia, email: Michael.Schuliga@newcastle.edu.au

ABSTRACT

Senescence and mitochondrial stress are mutually reinforcing age-related processes that contribute to idiopathic pulmonary fibrosis (IPF); a lethal disease that manifests primarily in the elderly. Whilst evidence is accumulating that GMP-AMP synthase (cGAS) is crucial in perpetuating senescence by binding damaged DNA released into the cytosol, its role in IPF is not known. This study examines the contributions of cGAS and self DNA to the senescence of lung fibroblasts from IPF patients (IPF-LFs) and healthy controls (Ctrl-LFs). cGAS immunoreactivity was observed in regions of fibrosis associated with fibroblasts in lung tissue of IPF patients. Pharmacological inhibition of cGAS or its knockdown by silencing RNA (siRNA) diminished the escalation of IPF-LF senescence in culture over 7 days as measured by decreased p21 expression, histone 2AXγ phosphorylation and/or IL-6 production ($P<0.05$, n=5-8). The targeting of cGAS also attenuated etoposide-induced senescence in Ctrl-LFs ($P<0.05$, n=5-8). Levels of mitochondrial DNA (mDNA) detected by qPCR in the cytosol and medium of IPF-LFs or senescence-induced Ctrl-LFs were higher than Ctrl-LFs at baseline ($P<0.05$, n=5-7). The addition of DNAse I (100 U/mL) deaccelerated IPF-LF senescence ($P<0.05$, n=5), whereas ectopic mDNA or the induction of endogenous mDNA release augmented Ctrl-LF senescence in a cGAS-dependent manner ($P<0.05$, n=5). In conclusion, we provide evidence that cGAS reinforces lung fibroblast senescence involving damaged self DNA. The targeting of cGAS to supress senescent-like responses may have potential important therapeutic implications in the treatment of IPF.

INTRODUCTION

IPF is a lethal lung disease that increases in incidence with advancing age; characterised by an excessive fibrosis that impedes gas exchange [1]. Of unknown aetiology, IPF is considered to be a consequence of a dysregulated repair response of epithelial origin [2]. The pharmacological therapies currently used to treat IPF at best slow disease progression in some patients, do not reverse fibrosis, are expensive and have significant side-effects [3, 4]. Due to the slow onset and nature of symptoms, the fibrosis at the time of diagnosis is firmly entrenched and self-perpetuating and as such, the most feasible approach to treating IPF is to target the triggers of the ongoing fibrosis. Recent studies show that premature senescence in alveolar epithelial cells (AECs) and lung fibroblasts (LFs) underlie key pathological changes in IPF such as a highly activated secretome, impaired re-epithelialisation and fibroblast persistence [5, 6]. All of which strongly supports a key role for senescence in the pathogenesis of IPF.

Senescence is the outcome of a DNA damage response (DDR) and a subsequent series of processes that ultimately lead to stable cell cycle arrest [7]. Telomere shortening, mitochondrial dysfunction and oncogenic signalling are underlying causes of the DDR [8-10]. Aside from cell cycle arrest, senescent cells are resistant to apoptosis, and have significant paracrine activities crucial for many facets of normal development and tissue function as well as pathologies including fibrosis [11]. Senescent cells are highly secretory, driving a range of different functions through the senescence-associated secretory phenotype (SASP). Senescent-linked biomarkers, specifically telomere shortening and the accumulation of senescent cells in the lung implicate a role of senescence in age-related chronic lung diseases such as IPF and chronic obstructive pulmonary disease (COPD) [12, 13]. Senescence in lung epithelial cells in particular has been proposed to be the crux of the

aberrant wound healing response observed in these diseases; possibly by hindering re-epithelialisation (and/or by the activation of resident fibroblasts) [6, 14-16]. Indeed, senescent epithelial cells in histological tissue sections from IPF and COPD lung are a well-documented feature of these diseases [12, 14, 17, 18]. Furthermore, the targeted removal of senescent epithelial cells with senolytic compounds attenuates SASP mediators and ECM markers, while increasing expression of alveolar epithelial markers *ex vivo* [14, 18]. Additionally, exposure to cigarette smoke, an important risk factor for both IPF and COPD induces AEC senescence in vitro [19]. Fibroblasts from the lung parenchyma and airways of IPF and COPD patients respectively also display multiple features of senescence *in vivo* and *in vitro* and significantly more so than age-matched controls. For example, telomeres are shortened, expression of the cyclin dependent kinases inhibitors $p21^{waf1}$ and $p16^{ink4D}$ is increased, as is the production of SASP mediators such as IL-6, MCP-1, CCL5 and urokinase [20-22]. A failure to eliminate senescent fibroblasts by apoptosis or immune cell clearance may also impede wound resolution and contribute to disease progression in IPF and COPD [16, 17, 23].

DNA released from the nucleus or mitochondria as a consequence of aging, injury, infection and other stresses can be a potent damage associated molecular pathogen (DAMP) capable of triggering autocrine and paracrine inflammatory response by activating inflammasomes (in particular NLRP3) or toll-like receptors (ie TLR9) and other DNA binding receptors (ie cyclic GMP-AMP synthase [cGAS]) of the innate immune system [24]. Indeed, the cGAS-STING (stimulator of interferon genes) signaling axis has emerged as a crucial regulator of type I IFN and nuclear factor-kappa-B (NF-κB) p65 responses to both exogenous and endogenous DNA. The enzyme cGAS detects DNA in the cytoplasm to generate the cyclic dinucleotide cGAMP, which serves as a second messenger that binds and activates STING.

This in turn leads to the activation of NF-κB and interferon regulatory factor 3 (IRF3) which triggers pro-inflammatory and type I IFN responses with both an autocrine and paracrine impact. Recent studies suggest a molecular link exists between DNA damage, the SASP and senescence involving the cGAS-STING pathway [25]. Whether this link drives fibrosis in IPF is still not known. However, IPF-LFs release increased levels of mitochondrial DNA (mDNA) in culture supernatants as compared to LFs from age-matched controls *in vitro* [26]. Furthermore, extracellular mDNA in the BALF/serum of IPF patients predicts all-cause mortality [26]. The mechanisms of the increased mDNA release, and its temporal impact on neighbouring cells remains unknown.

In this study, we investigate whether the increased release of self (m)DNA by LFs is a consequence of senescence, and whether this DNA reinforces and/or facilitates the spread of senescence by its actions on naïve lung cells in a manner involving cGAS. To address this, we used LFs isolated from IPF patients (IPF-LFs) with high baseline senescence, or in cells from control donors (Ctrl-LFs) that were induced to become senescent using etoposide. The levels of cytosolic and extracellular DNA formed by these cells were examined, as well as the effect of targeting cGAS on the senescent phenotype. The role of self DNA in cGAS-mediated paracrine senescence was investigated by exposing naïve Ctrl-LFs to exogenous mDNA (of fibroblast origin) or IPF-LFs to ectopic DNAseI. Furthermore, the knockdown of the mDNA packaging protein, mitochondrial transcription factor A (TFAM) was used to induce mDNA release in order to delineate the contribution of endogenous mDNA to LF senescence.

MATERIALS AND METHODS

Lung tissue and establishment of cell culture

LF cultures were established using lung tissue resections from patients at the John Hunter Hospital (New Lambton Heights, Australia) under ethical approval from the Hunter New England Human Research Ethics Committee (16/07/20/5.03) following guidelines from the National Health and Medical Research Council (NHMRC, Australia). All patients had provided written, informed consent. LF cultures were also obtained from the Alfred Lung Fibrosis Biobank (Alfred Hospital, Melbourne, Australia) under ethical approval from the Alfred Health Ethics Committee (#336/13) following NHMRC guidelines. Donors were classified as either IPF or Control (Ctrl). IPF patients were accurately phenotyped by respiratory clinicians in regards to underlying diagnosis and disease severity. Age-matched controls were either patients with no evidence of interstitial lung disease (ILD) undergoing routine thoracic surgical procedures or lung transplant donors. LFs in culture were established as described previously [27]. Cultures from separate patients/donors were used at an early passage (3-7) to minimize complications with replicative senescence.

Cell culture conditions and treatments

LFs were grown in Dulbecco's Modified Eagles Medium (DMEM) containing low glucose (1 g/L), L-alanyl-glutamine (4 mM), sodium pyruvate (1 mM), non-essential amino acids (1% v/v, Sigma) and heat-inactivated fetal calf serum (FCS, 10% v/v, Interpath) at 37°C in air containing 5% CO_2. Treatments including RU.521 (3 μM, Aobious), DNaseI (100 U/mL, Sigma), ectopic DNA (0.5 ng/mL) and DNA or cGAMP (10 μg/mL) complexed with Lipofectamine 3000 (Invitrogen) were added to the culture medium 24 hours after cells were seeded into 6, 12, 24 or 48 well plates (2 x 10^4 cells/cm^2) and re-added with each subsequent medium change (every 2-3 days) over a 7 day period. DNA and cGAMP were complexed

with Lipofectamine to facilitate cell entry and prepared as described by Aarreberg *et al* [28]. For etoposide- and rotenone-induced senescence experiments, Ctrl-LFs were replenished in serum-reduced DMEM containing 0.4 % v/v FCS the day after seeding (3 x 10^4 cells/cm^2) and 24 h before the addition of etoposide (10 μM), rotenone (100 nM) or the appropriate volume of DMSO as vehicle control. After 24 h incubation with etoposide, the media was replenished with fresh serum-reduced medium. RU.521 was added 30 min before etoposide, and re-added with each subsequent medium change (every 2-3 days) for a total of 5 days after the addition of etoposide.

siRNA transfection

Cells grown in 12, 24 or 48 well plates were transfected with 20 nM RNA short interference (siRNA) duplex oligonucleotides using RNA*i*Max Lipofectamine (Invitrogen, CA, USA) according to the manufacturer's instructions. Prior to transfection (24 h after seeding at 2 x 10^4 cells/cm^2) cells were replenished in antibiotic-free serum containing DMEM, before incubation with siRNA-Lipofectamine complex for 6 h. The media was then replaced with DMEM containing serum and antibiotics, before cells were maintained for an additional 7 days in culture with subsequent media changes every 2-3 days. cGAS, TFAM and control siRNA (Sigma-Aldrich, MO, USA) were used in the study. Two duplexes of cGAS siRNA were used at a 1:1 ratio: GCUACUAUGAGCACGUGAA[dT][dT]; and GCUGUAACACUUCUUAUUA[dT] [dT]-3' (only sequences of the sense strand for each duplex are provided). One duplex of TFAM siRNA was used: GGCAAGUUGUCCAAAGAAA[dT][dT]. For experiments where Ctrl-LFs were transfected with cGAS siRNA, etoposide was added once, 24 hours following transfection. For Ctrl-LFs transfected with TFAM, RU.521 was added after the addition of siRNA-Lipofectamine complex and re-added with each subsequent medium change.

Immunohistochemistry (IHC)

Paraffin-embedded sections of human parenchymal lung tissue were immunohistochemically stained for cGAS antigen. Antigen was identified by rabbit polyclonal antibodies to cGAS (#15102, Cell Signaling Technology). Antibody staining was completed using the Dako EnVision anti-rabbit kit as appropriate (Dako Corp., Carpinteria, CA, USA) and 3,3'-diaminobenzidine (Sigma-Aldrich, St Louis, MO, USA); where sections were counterstained with hematoxylin.

Purification of mDNA

IPF-LFs grown to confluence in T75 tissue culture flasks were harvested by trypsinization before being washed in PBS. Cells were pelleted by centrifugation at 300 *g* before mitochondria were isolated using the Mitochondrial Isolation Kit for Cultured Cells (ThermoScientific) according to the Manufacturer's instruction. DNA was extracted from mitochondria using QIAamp DNA mini spin columns (Qiagen).

Immunofluorescence

Phosphorylated histone 2AX (γH2AX) and NF-κB p65 (or RelA), a NF-κB family member and a subunit of the NF-κB transcription factor complex were detected in LFs in culture by immunofluorescence. Cells grown in 48-well plates were fixed with 4% w/v formaldehyde in PBS for 10 min before blocking and permeabilization with 0.15% v/v Triton X-100, 10% v/v goat serum and 1% w/v BSA in PBS for 10 min. Cells were then incubated with anti-phospho-γH2AX (Ser139) (#9718, Cell Signaling Technology) or -NF-κB p65 (#8242S, Cell Signaling Technology) rabbit polyclonal IgG overnight at 4^{o}C. After washing, cells were incubated with Alexa Fluor 555 anti-rabbit-conjugate (#4408, Cell Signaling Technology) for

1 h at room temperature. All antibodies were used at a 1 in 200 dilution. Cells were counterstained with DAPI (1 μg/mL, Sigma) and mounted in 70% v/v glycerol. Fluorescent images of 2-3 randomly selected microscopic fields (100-400 cells) of each treatment group were taken at 100 X magnification using a Nikon Eclipse Ti-U fluorescence microscope. For each image, the fluorescence of the red and blue channels were pseudo-colored and merged using ImageJ software (NIH). Quantitation was achieved with Fiji software (NIH) using macro plugins to specifically measure the percentage area of nucleus associated with fluorescence from either γH2AX or NF-κB p65.

Senescence-associated β-galactosidase detection

For senescence-associated *β* -galactosidase (SA-*β*-Gal) staining, cell cultures in 12 well plates were fixed and stained using a commercial kit (Cell Signaling Technology) according to the manufacturer's instructions. Cells were counterstained with DAPI (1 μg/mL, Sigma) before both light microscopy and fluorescence images were taken at 100 X magnification using a Nikon Eclipse Ti-U inverted fluorescence microscope. Photos of 2-3 randomly selected microscopic fields were taken for each treatment group and the number of SA-*β*-Gal positive cells and DAPI-stained nuclei (100-400 per field of view) were counted.

ELISA and protein assays

Levels of IL-6 in LF supernatants were measured by specific sandwich enzyme-linked immunosorbent assays (ELISA) using commercial kits (RnDSystems, MN, USA) as according to the manufacturer's instructions. Protein concentration in cell lysates were measured using the BCA assay kit (Thermo Scientific).

Preparation of cytosolic and whole cell extracts

Media was removed from cells before being harvested by trypsinisation and resuspended in PBS. Any floating cells or debris in the media was removed by centrifugation. One tenth of the trypsinized cells (100 μL) was combined with 800 μL of 50 μM NaOH before heating at 100^{o}C for 30 min, then neutralisation by the addition of 100 μL 1M Tris-HCl pH 8. Denatured whole cell extracts allow levels of DNA detected in the cytosol fraction (and medium) to be normalised to total DNA. The remaining 900 μL cell suspension was centrifuged at 300 *g* to pellet the cells before sub-cellular fractionation using the Mitochondrial Isolation Kit for Cultured Cells (ThermoScientific) according to the Manufacturer's instruction. The kit allows for the isolation of a cytosol fraction free of nuclei and mitochondria. Pellets of the latter were combined and used as a positive control for nuclear and mitochondrial protein in assessing the purity of the cytosol fraction by Western blotting.

PCR analysis

Real time polymerase chain reaction (PCR) was conducted to quantify nucleic acids. RNA and DNA were purified from cells and/or from subcellular fractions (ie cytosol and media) using RNeasy and QIAamp DNA mini spin columns (Qiagen) respectively. RNA was reverse transcribed into cDNA using the iScript Advanced cDNA kit (BioRad). DNA was amplified by PCR using the iTaq Universal SYBR Green Supermix (BioRad) in an ABI Prism 7500HT sequence detection system (Applied Biosystems) with the relevant PCR primers: 18S rRNA FP ATCGGGGATTGCAATTATTC and RP CTCACTAAACCATCCAATCG; β2-microglobulin (B2M) FP AAGGACTGGTCTTTCTATCTC and RP GATCCCACTTAACTATCTTGG ; CDKN1A (p21) FP CAGCATGACAGATTTCTACC and RP CAGGGTATGTACATGAGGAG; cGAS FP ATCTGTGGATATAACCCTGG and RP TCTTGGAAACCATTTCCTTC; TFAM

FP GAAAGATTCCAAGAAGCTAAGG and CGTCCAACTTCAATCATTTG; and $tRNA^{Leu(UUR)}$ FP CACCCAAGAACAGGGTTTGT and RP TGGCCATGGGTATGTTGTTA. For RNA quantitation, the threshold cycle (CT) value determined for each gene of each sample was normalized against that obtained for the internal control, 18S rRNA. The level of mRNA for a particular gene is proportional to $2^{-(\Delta CT)}$, where ΔCT is the difference between the CT values of the target and control. Relative levels ($2^{-(\Delta CT)}$) of mDNA in the cytosol fraction and media were measured using PCR primers for the mitochondrial gene, $tRNA^{Leu(UUR)}$ and normalized to levels of tRNA-$Leu^{(UUR)}$ in whole cell extracts. Likewise, genomic DNA (gDNA) was measured using PCR primers for the nuclear gene, β2-microglobulin (B2M).

Immunoblotting

Cell lysates (10 μg protein) or equivalent volumes of cytosol and nuclear + mitochondrial combined fractions were subjected to SDS polyacrylamide gel electrophoresis (SDS-PAGE) using 4-15% Mini-Protean TGX 15 well stain free gels (BioRad). Fluorescent detection of protein after electrophoresis was imaged using a BioRad Gel Doc imaging system. Gels were then electroblotted as described previously [29] before membranes were cut and blocked with 1.5% v/v BSA and 2.5% skim milk in TBS-T (10 mM Tris; 75 mM NaCl; 0.1% Tween-20; pH 7.4) for 1 h. Membranes were incubated overnight at 4°C with rabbit polyclonal IgGs raised against cGAS (#15102, Cell Signaling Technology) or Lamin A/C (#2032, Cell Signaling Technology), goat polyclonal IgGs raised against GAPDH (#ab9483, Abcam) or mouse monoclonal antibodies raised against COX IV (#11967, Cell Signaling Technology). Blots were washed with TBS-T prior to incubation with the appropriate species specific IgG-horse raddish peroxidase conjugate (Chemicon, diluted 1:4000) for 1 h at room temperature.

Antigen was detected by enhanced chemiluminescence (Amersham Biosciences, UK) using a BioRad Gel Doc imaging system.

Superoxide measurement

To detect levels of mitochondrial-derived superoxide, lung fibroblasts grown in 96 well plates were replenished in phenol-red free DMEM before staining with MitoSOX (1 μM, Molecular Probes) for 20 min at 37^{o}C. Stained cells were analysed using a FLUOstar OPTIMA microplate reader (BMG Labtech). The excitation and emission wavelengths for MitoSOX were 485 and 590 nm respectively.

Statistical analysis

Data are presented as the mean ± SEM where *n* represents individual experiments conducted using cells from separate donors. Comparisons between two groups were analysed by the non-parametric Wilcoxon matched pairs signed rank or Mann-Whitney U tests (Graphpad Prism 5.0, Graphpad, San Diego, CA) where appropriate. A value of $P<0.05$ was considered to be statistically significant.

RESULTS

cGAS expression is increased in IPF

IHC shows cGAS antigen (brown) is associated with flattened elongate mesenchymal cells, comprising fibroblasts and smooth muscle cells, as well as cuboidal epithelial cells in the fibrotic lung of three IPF patients *in vivo* (**Fig. 1).** cGAS detection in lung section from two additional IPF patients are presented in the online supplement (**Fig. S1)**. cGAS antigen was sparsely detected in the structural cells of lung tissue from control donors, which are mainly alveolar epithelial cells (types I and II) (**Fig. 1 & Fig. S1)**. The levels of cGAS in cell lysates of IPF-LFs *in vitro* as detected by immunoblotting were significantly higher than age-matched Ctrl-LFs of equivalent passage ($P<0.05$, n=5-7) (**Fig. S2, supplement**).

Targeting cGAS diminishes the escalation of IPF-LF senescence

Inhibiting cGAS in IPF-LFs with RU.521 (3 μM) diminished the escalation of replicative senescence in culture. The exposure of IPF-LFs during exponential growth to RU.521 reduced levels of p21 and p16 mRNA and γH2AX within the nucleus when compared to the vehicle control after 7 d (**Fig. 2a-c**) ($P<0.05$, n=6-8). Cytochemical staining also suggests the activity of senescence-associated β-galactosidase (SA-β-gal) was reduced by RU.521 (**Fig. 2d**). In this study, the images of SA-β-Gal stained cells represent 3 or more separate experiments, with quantitative data presented in **Table S1** (supplement). Immunofluorescence detection also shows diminished levels of NF-κB p65 and its nuclear localisation in IPF-LFs are reduced following incubation with RU.521 (**Fig. 2e**) ($P<0.05$, n=5). Furthermore, a reduction in the levels of IL-6 protein and IL-6 and CCL2 mRNA (albeit not IL-8 mRNA) provides evidence that RU.521 has an impact on the SASP of IPF-LFs (**Fig. 2f-i**) ($P<0.05$, n=5). The knockdown of cGAS by siRNA transfection had an effect comparable to cGAS pharmacological inhibition on markers of senescence, including levels

of p21 and p16 mRNA, nuclear γH2AX and SASP expression in IPF-LFs (**Fig. 2j-r**) (P<0.05, n=5-8).

Targeting cGAS attenuates etoposide-induced Ctrl-LF senescence

To examine the role of cGAS in the acquisition of stress-induced LF senescence, we used Ctrl-LFs. This phenotype of cells, which have a lower baseline senescence than IPF-LFs, exhibit heightened senescence following treatment with etoposide [21]. Incubation of Ctrl-LFs with RU.521 attenuated etoposide (Etop, 10 μM)-induced increases in markers of senescence including levels of p21 and p16 mRNA, nuclear γH2AX and NF-κB p65 and SASP gene expression (**Fig. 3a-i**) (P<0.05, n=5-8). Similarly, suramin (50 μM), another pharmacological inhibitor of cGAS or transfection with cGAS siRNA attenuated chemical-induced Ctrl-LF senescence (**Fig. S3 & S4, supplement**) (P<0.05, n=5). Conversely, transfection of Ctrl-LFs with cGAMP, the enzymatic product of cGAS and the activator of STING induced Ctrl-LF senescence (**Fig. S5, supplement**) (P<0.05, n=5).

mDNA release increases in senescent fibroblasts

Levels of mDNA and genomic DNA (gDNA) in sub-cellular fractions of LFs were measured by qPCR using primers for $tRNA^{Leu(UUR)}$ and B2-microglobulin respectively [30]. Levels of mDNA were higher in both the cytosol and extracellular space of IPF-LFs when compared to Ctrl-LFs (**Fig. 4a**) (P<0.05, n=5-7). Whilst there were apparent increases in the levels of gDNA in the same IPF-LF fractions, the changes were not significant (**Fig. 4b**) (P>0.05, n=5-7). Inducing Ctrl-LFs to become more senescent with etoposide also increased the release of mDNA into the cytosol and extracellular space (**Fig. 4c**) (P<0.05, n=6). Etoposide had a similar effect on the level of gDNA in Ctrl-LF cytosol (**Fig. 4d**) (P<0.05, n=6). Immunoblots of cytosol from Ctrl-LFs at baseline were used to assess the purity of these fractions after

isolation, showing negligible contamination by nuclear or mitochondrial protein (laminin A/C and CoxIV respectively) (**Fig. 4e**).

Extracellular mDNA mediates fibroblast senescence in a cGAS-dependent manner

Recently, ectopic mDNA (0.5 ng/mL) was shown to induce fibrogenic responses in LFs, but parameters of senescence were not assessed, nor the mechanism by which mDNA elicits its fibrogenic actions [26]. Here, the addition of DNAse I (100 U/mL, 7d) diminished the escalation of replicative senescence in IPF-LFs, suggesting that increased levels of extracellular self DNA may mediate secondary senescence in autocrine and/or paracrine manners (**Fig. 5a-h**) ($P<0.05$, n=4-6). Furthermore, the addition of 'naked' mDNA or gDNA (0.5 ng/mL, 7 d) to the media of Ctrl-LFs induced increases in the senescent markers, p21 expression and IL6 production (**Fig. 6a-b**) ($P<0.05$, n=5). Transfection of Ctrl-LFs with the same amount of mDNA using Lipofectamine3000 also induced increases in these same senescent markers. There was no significant difference between mDNA and gDNA or mDNA-transfection complex in regards to either parameter analysed; albeit the latter appeared to be the most effective in inducing IL-6 production. The effect of ectopic mDNA on Ctrl-LF senescence, as measured by increases in the levels of p21 mRNA, nuclear γH2AX and NF-κB p65, SA-β-Gal activity and SASP expression was sensitive to cGAS inhibition (**Fig. 6c-j**) ($P<0.05$, n=5).

mDNA stress and release induce Ctrl-LF senescence in a cGAS-dependent manner

To delineate the specific contribution of endogenous mDNA release in cGAS activation and senescence, Ctrl-LFs were transfected with siRNA targeting the mitochondrial transcription factor A (TFAM). A reduction in TFAM, a mDNA packaging protein contributes to mDNA release [31]. The knockdown of TFAM mRNA was shown two days following TFAM transfection, as was an increase in the level of mDNA detected in the cytosol (**Fig. 7a-b**)

(P<0.05, n=5). Levels of senescent markers including p21 mRNA were higher in Ctrl-LFs 7 d after transfection with TFAM than Ctrl siRNA (**Fig. 7c-f**) (P<0.05, n=5-6). Increases in IL-6 production and SASP gene expression were accompanied by increases in the levels and nuclear localisation of NF-κB p65 in TFAM siRNA transfected cells. RU.521 attenuated TFAM siRNA-induced Ctrl-LF senescence and NF-κB nuclear translocation (**Fig. 7c-f**) (P<0.05, n=5-6).

cGAS inhibition attenuates rotenone-induced LF senescence

Senescence and mitochondrial dysfunction are highly interrelated processes that can drive/sustain one another. To explore the contribution of mitochondrial dysfunction to cGAS-mediated senescence, Ctrl-LFs were treated with rotenone; an inhibitor of complex I of the mitochondrial respiratory chain and inducer of Ctrl-LF senescence [21]. In this study, we show rotenone-induced senescence of Ctrl-LFs, as measured by increased levels of p21 and p16 mRNA, nuclear γH2AX and IL-6 production is attenuated either by incubation with RU.521 (**Fig. 8a-d**) (P<0.05, n=5) or transfection with cGAS siRNA (**Fig. 8e-h**) (P<0.05, n=5). The effects of rotenone on senescence corresponded to increased levels of mDNA detected in the cytosol of LFs (**Fig. S6**, **supplement**). Targeting cGAS by pharmacological inhibition not only diminished the levels of cytosolic mDNA detected in either rotenone- or etoposide-treated Ctrl-LFs, but also other parameters of mitochondrial dysfunction including increased ratios of mDNA/gDNA (a surrogate measure of mitochondrial biogenesis) and elevated levels of mitochondrial-derived superoxide (**Fig. S6**, **supplement**) (P<0.05, n=5-6).

DISCUSSION

Whilst the DNA sensor cGAS is crucial in cellular senescence and aging, its roles in IPF have not yet been reported. In this study, cGAS antigen was detected in lung tissue of IPF patients, primarily associated with mesenchymal cells. Targeting cGAS in IPF-LFs *in vitro* diminished the escalation of senescence, implicating cGAS as a sensor of cytosolic damaged DNA in LF senescence. In support, cGAS inhibition also attenuated etoposide-induced Ctrl-LF senescence. We also provide evidence that mDNA release is a feature of LF senescence by showing that the levels of mDNA detected in the cytosol and extracellular space of senescent-prone IPF-LFs or etoposide-treated Ctrl-LFs were higher than Ctrl-LFs at baseline. Furthermore, ectopic mDNA or TFAM knockdown (which elicits mDNA release) augmented Ctrl-LF senscence in a cGAS-dependent manner. Finally, ectopic DNAseI decelerated IPF-LF senescence, suggesting a contribution of extracellular DNA to autocrine and/or paracrine senescence. Collectively our data indicates a cGAS-dependent response links LF DNA damage and senescence in IPF.

Well recognised for its important role in innate immunity by sensing bacterial and viral DNA of infecting pathogens, cGAS also binds and is activated by damaged endogenous DNA released from the nucleus and mitochondria [25, 31]. The binding of double stranded DNA (dsDNA), regardless of sequence or modification to cytosolic cGAS generates cGAMP to activate STING. For the human enzyme, unlike the mouse equivalent, cGAS activation is dependent on the length of the DNA substrate; with longer dsDNA being more efficacious than shorter forms in facilitating cGAMP synthesis [32]. Cell autonomous DNA-driven inflammation involving cGAS is critical in many diseases ranging from monogenic auto-inflammatory diseases such as Aicardi Goutières Syndrome to more complex multi-factorial age-related diseases, including myocardial infarction [33]. Recently, cGAS has also been

shown to be a crucial mediator of cellular senescence, which is an important feature of IPF pathology [25, 34]. However, the role of cGAS in IPF has not been evaluated to our knowledge. In this study, cGAS antigen was detected in mesenchymal cells in fibrotic IPF lung, with levels being higher in IPF-LFs than Ctrl-LFs *in vitro*. Furthermore, targeting cGAS pharmacologically (using RU.521 or suramin) or by genetic means (siRNA transfection) diminished the escalation of IPF-LF senescence and attenuated etoposide-induced Ctrl-LF senescence as assessed by concomitant decreases in p21 expression, IL-6 production, phosphorylation of H2AXγ and SA-β-gal activity. These parameters have previously been used in combination in the evaluation of cellular senescence [14, 21, 23, 25, 34]. Importantly, γH2AX is also a surrogate of nuclear DNA damage, being activated at dsDNA breaks in the nucleus as part of the DDR that initiates senescence [21]. It should be noted that γH2AX phosphorylation can also occur concurrently with DNA fragmentation in apoptosis; albeit its distribution in this process is diffuse, not the focal pattern associated with senescence [35]. Whilst the contribution of apoptosis cannot be excluded, we have shown for key experiments in this study that changes in the levels of nuclear γH2AX also correspond with changes in the percentage of cells that exhibit visible γH2AX nuclear foci (**Fig. S7**, supplement). Furthermore, it is well documented that lung fibroblasts from IPF patients exhibit resistance to apoptosis *in vitro*, suggesting apoptosis is unlikely to be a major contributor to the changes in the parameters of senescence that were measured in this study [36, 37]. Collectively, we provide evidence that cGAS contributes to LF senescence in IPF. Further analysis of lung tissue from IPF patients showing whether levels of cGAMP are elevated and/or the STING pathway is activated in senescent LFs *in vivo* would corroborate our findings and support a role of cGAS in IPF.

Damage to mDNA increases in frequency with oxidative stress and accumulates in tissues with ageing and in disease [38]. Base oxidation (ie 8-OHdG) and the 4977-bp mitochondrial deletion (ΔmtDNA4977) are modifications that reduce the physical association of mDNA with TFAM contributing to mDNA release [31]. Cytosolic mDNA is a potent damage DAMP, capable of triggering innate immune and inflammatory responses by binding PRRs, including cGAS [24, 28]. To our knowledge, there is no direct evidence in the literature that mDNA is a mediator of cGAS-dependent senescence, with previous studies implicating damaged nDNA as the primary activator of senescence [25, 34]. However, our data that shows increased levels of mDNA in both the cytosol and extracellular space of senescent LFs suggests mDNA is also likely to drive IPF-LF senescence. In support, ectopic mDNA, whether added 'naked' or transfected using Lipofectamine 3000, induced LF senescence in a cGAS-dependent manner. Furthermore, the knockdown of TFAM, which induces mitochondrial stress and release of endogenous mDNA contributed to cGAS-mediated LF senescence. Asides from mDNA packaging, TFAM serves as a transcriptional factor for mDNA genes; thus the protective effect of TFAM against senescence may also involve its other roles in regulating mitochondrial homeostasis. Regardless, collectively our data support a contribution of mDNA in LF senescence involving cGAS. Whether other PRRs (ie TLR9) are involved in LF senescence cannot be excluded, nor the involvement of gDNA, which we expect is most certainly the case. Levels of the latter in the cytosol of etoposide-treated Ctrl-LFs were also higher than at baseline and ectopic gDNA had an effect comparable to mDNA on LF senescence. It should be noted that TLR9 preferentially binds DNA with unmethylated CpG dinucleotides, as found within bacterial and mDNA, but rarely in gDNA. However, there is accumulating evidence from other studies that supports a potential role of TLR9 in IPF, including the observation that TLR9 is up-regulated in LFs from patients with rapidly progressive IPF when compared to stable IPF [39]. Furthermore,

TLR9 in the membrane of the A549 alveolar epithelial cell line has recently been shown to be activated by extracellular mDNA, triggering secretion of the pro-fibrotic factor TGF-β [40].

The contribution of cGAS in senescence involves STING activation and the subsequent induction of the transcription factors NF-κB and IRF3. In this study, immunofluorescence detection of the NF-κB subunit p65, particularly within the nucleus was increased in senescent LFs, including Ctrl-LFs treated with ectopic mDNA or following TFAM knockdown. These increases in NF-κB were diminished by incubation with the cGAS inhibitor RU.521. NF-κB is a pivotal regulator of the SASP that comprises an array of cytokines, chemokines and proteases that can mediate secondary senescence via autocrine and paracrine processes [34]. We have previously shown that the levels of p65 mRNA and protein are higher in IPF- than Ctrl-LFs, corresponding to increases in a broad range of inflammatory mediators and stimuli including IL-6; the archetypal SASP cytokine [21]. It is quite plausible that the effects of targeting cGAS on LF senescence involves the inhibition of NF-κB-regulated SASP cytokine expression. Whilst decreases in LF IL-6 production by RU.521 and cGAS siRNA support this premise, other SASP mediators were not analysed in this study, nor was the causal involvement of NF-κB in regulating the SASP and secondary senescence. Furthermore, the potential involvement of IRF3 and/or interferons in the relay of cGAS-mediated LF senescence were not investigated. However, we did not detect the IRF3-regulated type I interferon IFN-β in LF culture supernatants, regardless of treatment with etoposide (data not shown). Indeed, the expression of key regulators and mediators of interferon responses including IP10, IRF1 and IRF7 have been reported to be markedly suppressed in IPF-LFs when compared to Ctrl-LFs; suggesting that interferons do not contribute to cGAS-mediated LF senescence. Furthermore, senescent prone fibroblasts from patients with the premature aging disease Hutchinson-Gilford progeria syndrome (HGPS) or

mouse models of HGPS exhibit upregulation of the cGAS/STING cytosolic DNA sensing pathway and activation of robust NF-κB-mediated responses, even though these cells express little interferon [41, 42].

Our previous investigations with IPF- and Ctrl-LFs show a cyclical, mutually reinforcing relationship between senescence and mitochondrial dysfunction; a viscous circle involving increased production of mitochondrial-derived ROS [21, 43]. In these studies, senescent prone IPF-LFs or senescent-induced Ctrl-LFs exhibited features of mitochondrial dysfunction, including increased superoxide production. Originally described by Correia-Melo and colleagues in embryonic MRC-5 fibroblasts, superoxide and mTORC1 were also shown to be key mediators of IPF-lung fibroblast senescence; linking the DDR with alterations in mitochondrial homeostasis in an auto-amplifying loop that perpetuates senescence [44]. Our current data also suggests that mDNA and cGAS are potential mediators of this viscous circle. In particular, we show that senescent LFs release increased amounts of mDNA and pharmacological cGAS inhibition diminishes both senescence and mitochondrial dysfunction induced by etoposide or rotenone. It is plausible that in IPF, damaged mDNA released into the cytoplasmic and extracellular spaces by aging, dysfunctional mitochondria bind PRRs. In particular, cGAS activation in the cytosol by this self DNA evokes a 'sterile' inflammatory response that perpetuates secondary senescence. Not only are senescent LFs more resistant to apoptosis and produce more cytokines, key features of IPF pathology, they are also more contractile and express more wound-type collagens. Whilst the latter were not measured in this study, we and others have shown previously that senescent LFs from IPF patients exhibit myofibroblast-like features [21, 23, 45]. Overall, our current findings have added significance in understanding IPF pathology following the recent discovery that higher levels of extracellular mDNA occur in IPF and are

predictive of all-cause mortality [26]. Furthermore, increases in oxidation and damaged mDNA are detected in lung tissue of IPF patients [40]. We hypothesise that ageing, dysfunctional mitochondria are key to IPF pathology by perpetuating senescence through the release of damaged mDNA and cGAS activation. If correct, targeting the cGAS-STING signalling axis will disrupt this viscous cycle and decelerate LF, and possibly AEC senescence; and as a consequence, key processes in IPF that contribute to the aberrant wound repair that drives fibrosis. Although this study provides evidence that cGAS inhibition is potentially senotherapeutic by preventing the induction of lung fibroblast senescence and its spread (ie secondary senescence); it remains undetermined whether targeting cGAS actually modulates the phenotype (ie SASP) of already senescent cells. Whilst we expect this to be the case, additional experiments are required to test if cGAS-targeting therapeutics are truly 'senomorphic' in the context of lung fibrosis, or just prevent further accumulation of senescent cells.

The immense potential of senescence as a drug target option for IPF is epitomized by the numerous pre-clinical and clinical lung fibrosis studies that are evaluating senolytics, particularly the cocktail of dasatinib plus quercetin (DQ) [14, 18, 46]. However, there are potential issues using DQ long term, in particular regarding its specificity, and the effect of targeting already senescent cells in general. Therapeutics that target processes that lead to accelerated senescence, rather than established senescence, are likely to be more beneficial, with a lower risk profile. Highly selective and potent cGAS inhibitors may provide an alternative option as treatment for IPF by targeting the cGAS-STING axis to slow the onset of senescence [47]. The highly selective cGAS inhibitor RU.521 has been shown in this and other studies to be effective at low micromolar concentrations in inhibiting cGAS function in human cells [48, 49]. However, the potency of RU.521 for human cGAS based on cell free

assays is substantially reduced for DNA substrates of shorter length, which may limit its therapeutic potential *in vivo* [32, 50]. Recently, a new group of small molecules with improved efficacy for inhibiting human cGAS and with less discrimination for smaller DNA have been discovered [50]. Suramin, a treatment for river blindness, has also recently been shown to be a potent inhibitor of cGAS activation by displacing DNA from cGAS [51]. This action may explain why suramin blocks fibroblast activation in models of chronic kidney disease [52]. Importantly, due to its quite unique pharmacokinetics, suramin has long term effects *in viv*o, requiring only a single low dose (<10 mg/kg) weekly in mice to achieve its anti-fibrotic actions; a dosing regimen which is expected to be associated with minimal side effects [52]. Further exploration of pharmacological cGAS inhibitors in pre-clinical models of lung fibrosis is warranted. Alternative approaches to potentially slow down the onset of cGAS-mediated senescence would be to target either downstream mediators of cGAS (ie STING) or extracellular DNA. Recombinant DNAseI (Dornase alfa) is a cystic fibrosis (CF) therapy adjunct administered by inhalation that reduces the viscoelasticity of CF sputum by breaking down the high levels of extracellular, polyanionic DNA released by disintegrating neutrophils present after lung infections. DNaseI was recently shown to reduce pulmonary inflammation in a murine model of silicosis, another important fibrotic ILD [53]. We again caution that targeting cGAS (or extracellular DNA) may only prevent further accumulation of senescent cells, rather than suppress the secretome and/or fibrotic response of pre-existing senescent lung fibroblasts. If so, cGAS-targeting therapies are unlikely to reverse established fibrosis in diseases such as IPF. Regardless, these approaches may have some potential as treatments for IPF due to the progressive course of the disease.

In conclusion, we show that cGAS inhibition or knockdown diminishes the escalation of IPF-LF senescence and chemical-induced Ctrl-LF senescence. We also provide evidence that LF

senescence is associated with an increase in the release of mDNA, which reinforces senescence in a cGAS-dependent manner. Overall, our study suggests that damaged, self DNA activates cGAS to perpetuate fibroblast senescence and aging in IPF and other fibrotic lung diseases.

CLINICAL PERSPECTIVE

- There is accumulating evidence that the DNA-sensing enzyme, GMP-AMP synthase (cGAS) is an important mediator of cell autonomous DNA-driven inflammation and senescence; yet its role in idiopathic pulmonary fibrosis (IPF) and other fibrotic lung diseases is not known.

- In this study, we provide evidence that senescent-prone lung fibroblasts from IPF patients release increased levels of mitochondrial DNA (mDNA) into the cytosol and extracellular space and that this self DNA reinforces senescence in a cGAS-dependent manner.

- We propose that cGAS is potentially a central player in IPF pathology; connecting mitochondrial stress, sterile inflammation (involving cGAS activation by self DNA) and senescence. Outcomes of this study will increase our understanding of the pathobiology of senescence and mitochondrial dysfunction in IPF and provide the rationale for using agents that target cGAS as potential therapies.

ACKNOWLEDGEMENT

This work was supported by the NHMRC (Australia) research grant #1099569. Additional support was from the Lung Foundation of Australia David Wilson Scholarship. JK Burgess was supported by a Rosalind Franklin Fellowship from the University of Groningen and the European Union. We thank the patients, thoracic surgeons, respiratory clinicians, pathologists and medical staff at the John Hunter Hospital (Newcastle) and Alfred Hospital (Melbourne) in Australia for assistance in obtaining expertly phenotyped human lung tissue.

AUTHORS CONTRIBUTION Concept and design: DAK, MS; acquisition, analysis and interpretation of data: MS, JR, DWW, KECB, ATR, JJ, GW, AJ; and drafting the manuscript for intellectual content: DAK, MS, CG, JKB, CMP, SEM.

CONFLICTS OF INTEREST

The authors confirm that there are no conflicts of interest.

FIGURE LEGENDS

Figure 1. *cGAS is increased in lung of IPF patients.* Sections of parenchymal tissue from 3 IPF patients and 2 control donors immunostained for cGAS. Included is a negative IgG control of lung tissue from one of the IPF patients. The IPF sections show cGAS staining (brown) in flattened elongate mesenchymal cells, as well as cuboidal epithelial cells in fibrotic lung tissue. Scale bar in images = 50 micron.

Figure 2. *Targeting cGAS decelerates IPF-LF senescence.* (**a-r**) The effect of RU.521 (3 μM) or cGAS siRNA on the senescence phenotype of IPF-LFs after 7 d, as measured by changes in the levels of p21 and p16 mRNA, nuclear γH2AX, SASP gene expression, SA-β-Gal cytochemical staining and IL-6 protein in conditioned media The effect of targeting cGAS on levels of nuclear NF-kB p65 was also assessed. The knockdown of cGAS by siRNA was validated by decreases in the levels of cGAS mRNA and protein (representative immunoblot of cGAS shown). Included are representative fluorescence images of γH2AX (red), NF-κB p65 (red) and nuclei (blue) of LFs and cytochemical staining of SA-β-Gal (blue). Differences between two treatment groups were analysed by a Wilcoxon matched pairs signed rank test *P<0.05, **P<0.01 (n=5-8). Scale bar in images = 50 micron.

Figure 3. *Pharmacological cGAS inhibition attenuates etoposide-induced senescence of Ctrl-LFs.* (**a-i**) The effect of RU.521 (3 μM) on the senescence phenotype of etoposide-treated Ctrl-LFs after 5 d. Included are representative fluorescence images of γH2AX (red), NF-κB (red) and nuclei (blue) of LFs and cytochemical staining of SA-β-Gal (blue). Differences between two treatment groups were analysed by a Wilcoxon matched pairs signed rank test *P<0.05, **P<0.01 (n=5-8). Scale bar in images = 50 micron.

Figure 4. *IPF- and senescent-induced Ctrl-LFs release increased levels of mDNA.* (**a-b**) Levels of mDNA and gDNA as detected by qPCR for the genes encoding mt-tRNAleu$_{(UUR)}$ and β2-microglobulin (B2M) respectively, in the cytosol and media of IPF- and Ctrl-LFs. DNA levels are expressed as a percentage of total mt-tRNAleu$_{(UUR)}$ or B2M detected in cells. Data were analyzed by a Mann Whitney test (*P<0.05, n=5-7). (**c-d**) Levels of mDNA and gDNA in the cytosol and media of etoposide-treated Ctrl-LFs (10 μM, 3 d). Differences between two treatment groups were analysed by a Wilcoxon matched pairs signed rank test (*P<0.05, n=6). (**e**) Immunoblots of the cytosolic and the combined nuclear and mitochondrial fractions of Ctrl-LFs at baseline showing bands for laminin A/C, GAPDH and CoxIV; markers for the nucleus, cytosol + nucleus and mitochondria respectively.

Figure 5. *Ectopic DNAseI decelerates IPF-LF senescence.* IPF-LFs treated with DNAseI (50 U) for 7 d were evaluated for markers of senescence. **(a-e)** Levels of p21 and p16 mRNA, IL-6 protein and nuclear γH2AX. Shown are representative fluorescence images of γH2AX (red) and nuclei (blue) of LFs and cytochemical staining of SA-β-Gal (blue). **(f-h)** Levels of IL-6, CCL2 and IL-8 mRNA. Differences between two treatment groups were analysed by a Wilcoxon matched pairs signed rank test (*P<0.05, n=4-6). Scale bar in images = 50 micron.

Figure 6. *Ectopic DNA induces the senescence of Ctrl-LFs in a cGAS-dependent manner.* **(a, b)** Ctrl-LFs treated with mDNA and gDNA (0.5 ng/mL) for 7 d were evaluated for markers of senescence, p21 mRNA and IL-6 production. Cells were also transfected with the equivalent amount of mDNA complexed with lipofectamine3000 (LF-mDNA). **(c-g)** The combined effects of ectopic mDNA and RU.521 on Ctrl-LF senescence. Included are

representative fluorescence images ofγH2AX (red), NF-κB (red) and nuclei (blue) of LFs and cytochemical staining of SA-β-Gal (blue). **(h-j)** Levels of IL-6, CCL2 and IL-8 mRNA. Differences between two treatment groups were analysed by a Wilcoxon matched pairs signed rank test (*P<0.05, n=5-8). Scale bar in images = 50 micron.

Figure 7 *TFAM knockdown induces mDNA release and senescence in Ctrl-LFs in a cGAS-dependent manner.* (**a-f**) The effect of transfecting Ctrl-LFs with TFAM and Ctrl siRNA on levels of TFAM mRNA and mDNA in the cytosol (2d) and markers of senescence (7d). Differences between two treatment groups were analysed by a Wilcoxon matched pairs signed rank test, *P<0.05, (n=5-6). Scale bar in images = 100 micron.

Figure 8. *Targeting cGAS attenuates rotenone-induced LF senescence.* (**a-d**) The effect of RU.521 (3 μM) on the senescence phenotype of rotenone (100 nM)-treated Ctrl-LFs after 5 d, as measured by changes in the levels of p21 & p16 mRNA, nuclear γH2AX and IL-6 protein in conditioned media. (**e-h**) The effect of cGAS siRNA on the senescence phenotype of rotenone-treated Ctrl-LFs after 5 d. Differences between two treatment groups were analysed by a Wilcoxon matched pairs signed rank test, *P<0.05 (n=5-6). Scale bar in images = 50 micron.

REFERENCES

1. Murtha, L.A., et al., *The Processes and Mechanisms of Cardiac and Pulmonary Fibrosis.* Frontiers in Physiology, 2017. **8**: p. 777.
2. Ryu, J.H., et al., *Idiopathic pulmonary fibrosis: evolving concepts.* Mayo Clin Proc, 2014. **89**(8): p. 1130-42.
3. King, T.E., Jr., et al., *A phase 3 trial of pirfenidone in patients with idiopathic pulmonary fibrosis.* N Engl J Med, 2014. **370**(22): p. 2083-92.
4. Richeldi, L., et al., *Efficacy and safety of nintedanib in idiopathic pulmonary fibrosis.* N Engl J Med, 2014. **370**(22): p. 2071-82.
5. Waters, D.W., et al., *Fibroblast senescence in the pathology of idiopathic pulmonary fibrosis.* Am J Physiol Lung Cell Mol Physiol, 2018. **315**(2): p. L162-L172.
6. Murtha, L.A., et al., *The Role of Pathological Aging in Cardiac and Pulmonary Fibrosis.* Aging Dis, 2019. **10**(2): p. 419-428.
7. von Zglinicki, T., et al., *Human cell senescence as a DNA damage response.* Mech Ageing Dev, 2005. **126**(1): p. 111-7.
8. Passos, J.F., et al., *Feedback between p21 and reactive oxygen production is necessary for cell senescence.* Mol Syst Biol, 2010. **6**: p. 347.
9. d'Adda di Fagagna, F., et al., *A DNA damage checkpoint response in telomere-initiated senescence.* Nature, 2003. **426**(6963): p. 194-8.
10. Suram, A., et al., *Oncogene-induced telomere dysfunction enforces cellular senescence in human cancer precursor lesions.* EMBO J, 2012. **31**(13): p. 2839-51.
11. Herranz, N. and J. Gil, *Mechanisms and functions of cellular senescence.* J Clin Invest, 2018. **128**(4): p. 1238-1246.
12. Tsuji, T., K. Aoshiba, and A. Nagai, *Alveolar cell senescence in patients with pulmonary emphysema.* Am J Respir Crit Care Med, 2006. **174**(8): p. 886-93.
13. Armanios, M.Y., et al., *Telomerase mutations in families with idiopathic pulmonary fibrosis.* N Engl J Med, 2007. **356**(13): p. 1317-26.
14. Lehmann, M., et al., *Senolytic drugs target alveolar epithelial cell function and attenuate experimental lung fibrosis ex vivo.* Eur Respir J, 2017. **50**(2).
15. Naikawadi, R.P., et al., *Telomere dysfunction in alveolar epithelial cells causes lung remodeling and fibrosis.* JCI Insight, 2016. **1**(14): p. e86704.
16. Chilosi, M., et al., *Premature lung aging and cellular senescence in the pathogenesis of idiopathic pulmonary fibrosis and COPD/emphysema.* Transl Res, 2013. **162**(3): p. 156-73.
17. Hecker, L., et al., *Reversal of persistent fibrosis in aging by targeting Nox4-Nrf2 redox imbalance.* Sci Transl Med, 2014. **6**(231): p. 231ra47.
18. Schafer, M.J., et al., *Cellular senescence mediates fibrotic pulmonary disease.* Nat Commun, 2017. **8**: p. 14532.
19. Tsuji, T., K. Aoshiba, and A. Nagai, *Cigarette smoke induces senescence in alveolar epithelial cells.* Am J Respir Cell Mol Biol, 2004. **31**(6): p. 643-9.
20. Schuliga, M., et al., *Annexin A2 contributes to lung injury and fibrosis by augmenting factor Xa fibrogenic activity.* Am J Physiol Lung Cell Mol Physiol, 2017: p. ajplung 00553 2016.
21. Schuliga, M., et al., *Mitochondrial dysfunction contributes to the senescent phenotype of IPF lung fibroblasts.* J Cell Mol Med, 2018. **22**(12): p. 5847-5861.
22. Wrench, C., et al., *Small airway fibroblasts from COPD patients are senescent and pro-fibrotic.* European Respiratory Journal, 2018. **52**(suppl 62): p. PA2172.
23. Yanai, H., et al., *Cellular senescence-like features of lung fibroblasts derived from idiopathic pulmonary fibrosis patients.* Aging (Albany NY), 2015. **7**(9): p. 664-72.
24. West, A.P. and G.S. Shadel, *Mitochondrial DNA in innate immune responses and inflammatory pathology.* Nat Rev Immunol, 2017. **17**(6): p. 363-375.

25. Yang, H., et al., *cGAS is essential for cellular senescence.* Proc Natl Acad Sci U S A, 2017. **114**(23): p. E4612-E4620.
26. Ryu, C., et al., *Extracellular Mitochondrial DNA is Generated by Fibroblasts and Predicts Death in Idiopathic Pulmonary Fibrosis.* Am J Respir Crit Care Med, 2017.
27. Schuliga, M.J., et al., *Fibrillar collagen clamps lung mesenchymal cells in a nonproliferative and noncontractile phenotype.* Am J Respir Cell Mol Biol, 2009. **41**(6): p. 731-41.
28. Aarreberg, L.D., et al., *Interleukin-1beta Induces mtDNA Release to Activate Innate Immune Signaling via cGAS-STING.* Mol Cell, 2019.
29. Schuliga, M., et al., *Airway smooth muscle remodels pericellular collagen fibrils: implications for proliferation.* Am J Physiol Lung Cell Mol Physiol, 2010. **298**(4): p. L584-92.
30. Rooney, J.P., et al., *PCR based determination of mitochondrial DNA copy number in multiple species.* Methods Mol Biol, 2015. **1241**: p. 23-38.
31. West, A.P., et al., *Mitochondrial DNA stress primes the antiviral innate immune response.* Nature, 2015. **520**(7548): p. 553-7.
32. Zhou, W., et al., *Structure of the Human cGAS-DNA Complex Reveals Enhanced Control of Immune Surveillance.* Cell, 2018. **174**(2): p. 300-311 e11.
33. Li, T. and Z.J. Chen, *The cGAS-cGAMP-STING pathway connects DNA damage to inflammation, senescence, and cancer.* J Exp Med, 2018. **215**(5): p. 1287-1299.
34. Gluck, S., et al., *Innate immune sensing of cytosolic chromatin fragments through cGAS promotes senescence.* Nat Cell Biol, 2017. **19**(9): p. 1061-1070.
35. Rogakou, E.P., et al., *Initiation of DNA fragmentation during apoptosis induces phosphorylation of H2AX histone at serine 139.* J Biol Chem, 2000. **275**(13): p. 9390-5.
36. Huang, S.K., et al., *Histone modifications are responsible for decreased Fas expression and apoptosis resistance in fibrotic lung fibroblasts.* Cell Death Dis, 2013. **4**: p. e621.
37. Vuga, L.J., et al., *WNT5A is a regulator of fibroblast proliferation and resistance to apoptosis.* Am J Respir Cell Mol Biol, 2009. **41**(5): p. 583-9.
38. Lal, A., E. Gomez, and C. Calloway, *Increased mitochondrial DNA deletions and copy number in transfusion-dependent thalassemia.* JCI Insight, 2016. **1**(12).
39. Trujillo, G., et al., *TLR9 differentiates rapidly from slowly progressing forms of idiopathic pulmonary fibrosis.* Sci Transl Med, 2010. **2**(57): p. 57ra82.
40. Bueno, M., et al., *PINK1 attenuates mtDNA release in alveolar epithelial cells and TLR9 mediated profibrotic responses.* PLoS One, 2019. **14**(6): p. e0218003.
41. Kreienkamp, R., et al., *A Cell-Intrinsic Interferon-like Response Links Replication Stress to Cellular Aging Caused by Progerin.* Cell Rep, 2018. **22**(8): p. 2006-2015.
42. Osorio, F.G., et al., *Nuclear lamina defects cause ATM-dependent NF-kappaB activation and link accelerated aging to a systemic inflammatory response.* Genes Dev, 2012. **26**(20): p. 2311-24.
43. Waters, D.W., et al., *STAT3 Regulates the Onset of Oxidant-Induced Senescence in Lung Fibroblasts.* Am J Respir Cell Mol Biol, 2019.
44. Correia-Melo, C., et al., *Mitochondria are required for pro-ageing features of the senescent phenotype.* EMBO J, 2016. **35**(7): p. 724-42.
45. Alvarez, D., et al., *IPF lung fibroblasts have a senescent phenotype.* Am J Physiol Lung Cell Mol Physiol, 2017. **313**(6): p. L1164-L1173.
46. Justice, J.N., et al., *Senolytics in idiopathic pulmonary fibrosis: Results from a first-in-human, open-label, pilot study.* EBioMedicine, 2019. **40**: p. 554-563.
47. Vincent, J., et al., *Small molecule inhibition of cGAS reduces interferon expression in primary macrophages from autoimmune mice.* Nat Commun, 2017. **8**(1): p. 750.
48. Wang, R., et al., *Lipopolysaccharide enhances DNA-induced IFN-beta expression and autophagy by upregulating cGAS expression in A549 cells.* Exp Ther Med, 2019. **18**(5): p. 4157-4164.

49. McLemore, A., et al., *Genomic-DNA Exposed By Somatic Gene Mutations Engages the cGAS/STING Axis to License the NLRP3 Inflammasome in Myelodysplastic Syndromes.* Blood, 2018. **132**: p. 3075-3075.
50. Lama, L., et al., *Development of human cGAS-specific small-molecule inhibitors for repression of dsDNA-triggered interferon expression.* Nat Commun, 2019. **10**(1): p. 2261.
51. Wang, M., et al., *Suramin potently inhibits cGAMP synthase, cGAS, in THP1 cells to modulate IFN-beta levels.* Future Med Chem, 2018. **10**(11): p. 1301-1317.
52. Liu, N., et al., *Suramin inhibits renal fibrosis in chronic kidney disease.* J Am Soc Nephrol, 2011. **22**(6): p. 1064-75.
53. Benmerzoug, S., et al., *STING-dependent sensing of self-DNA drives silica-induced lung inflammation.* Nat Commun, 2018. **9**(1): p. 5226.

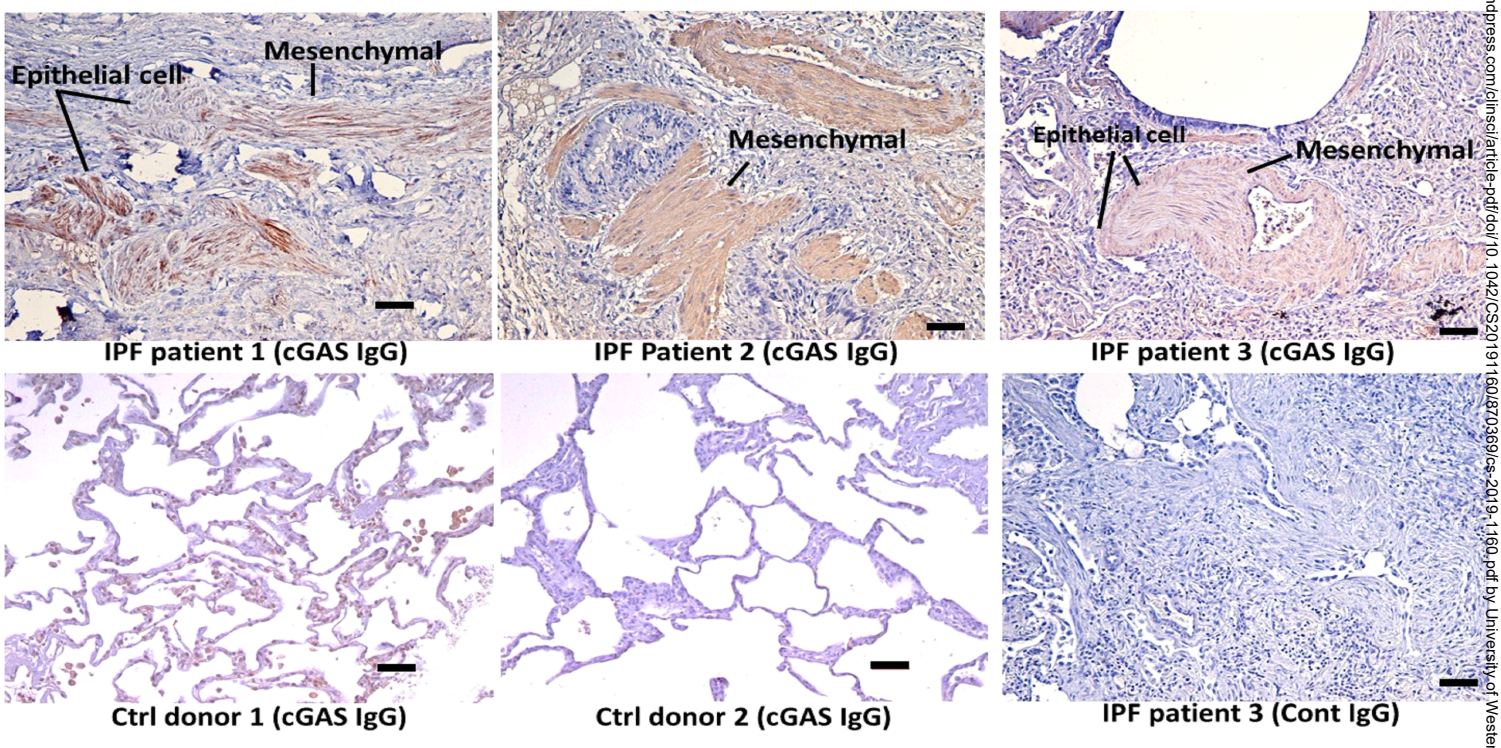

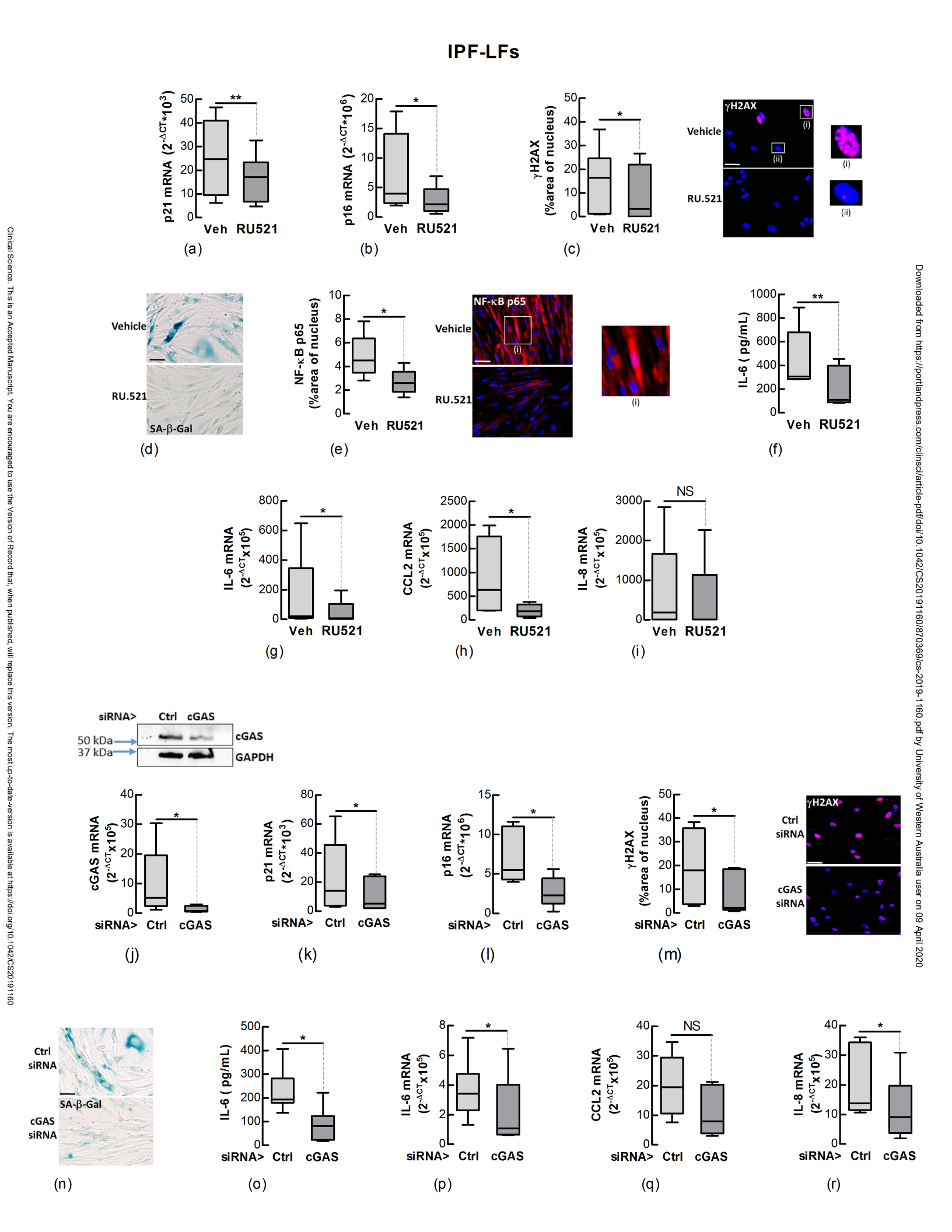

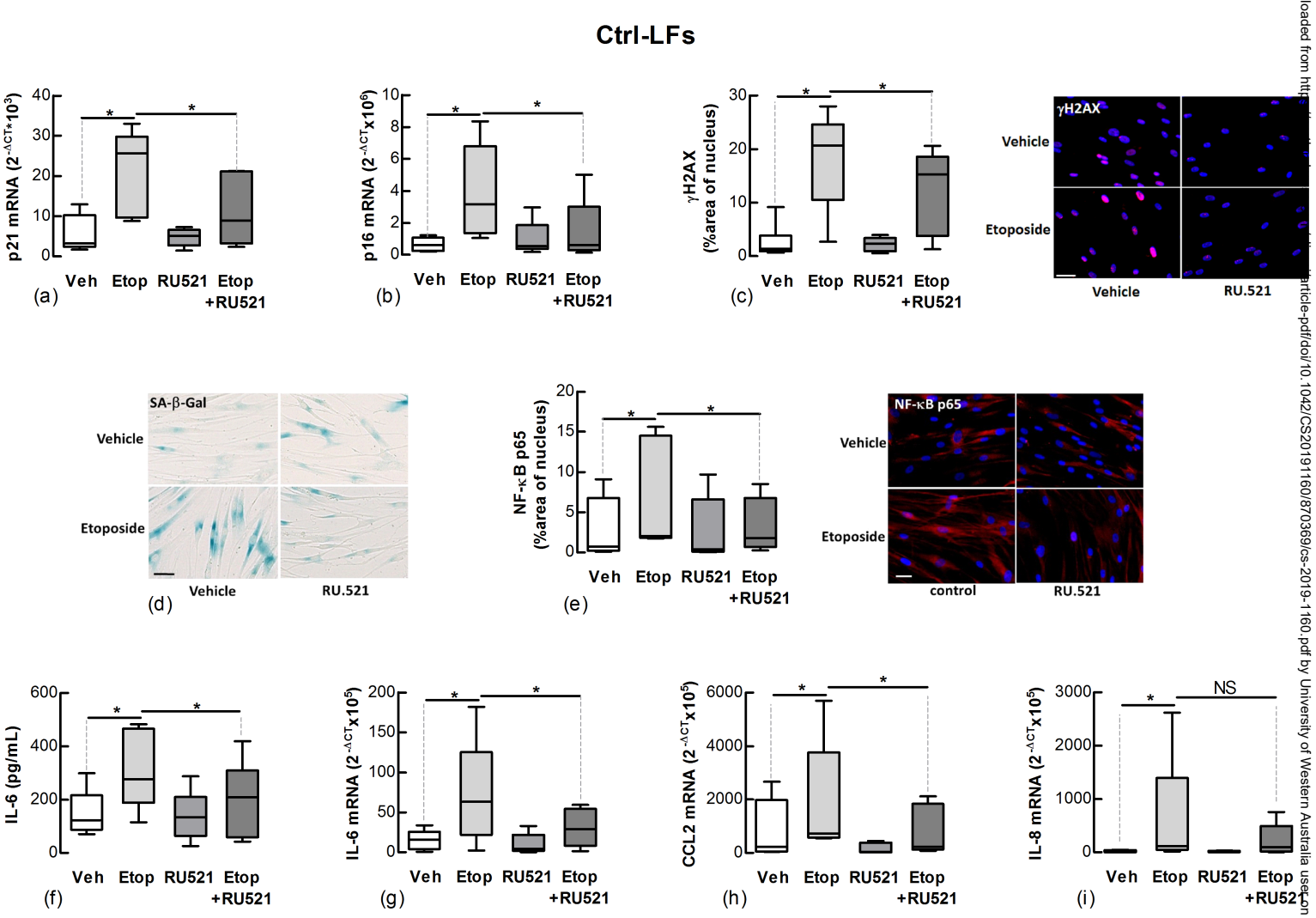

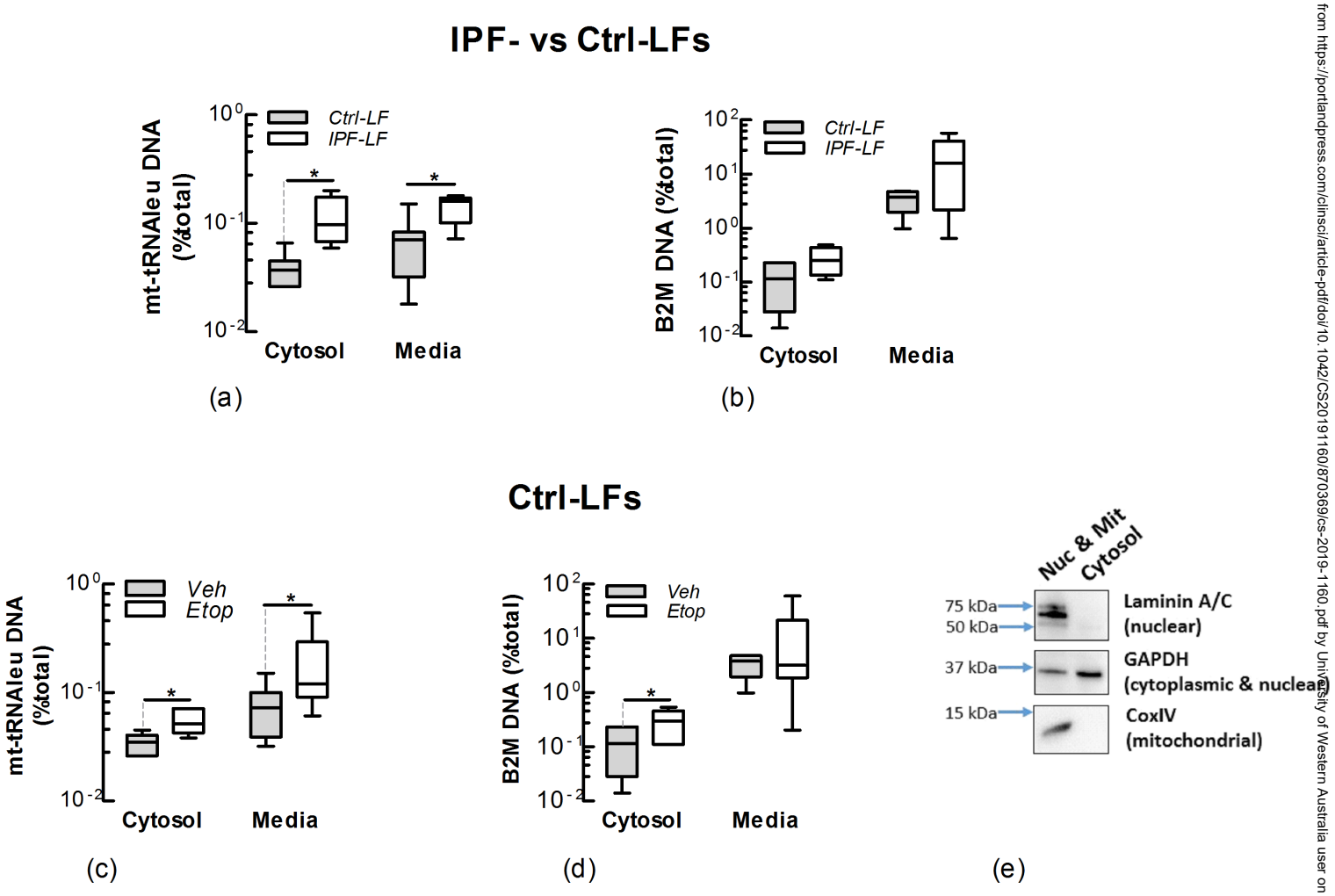

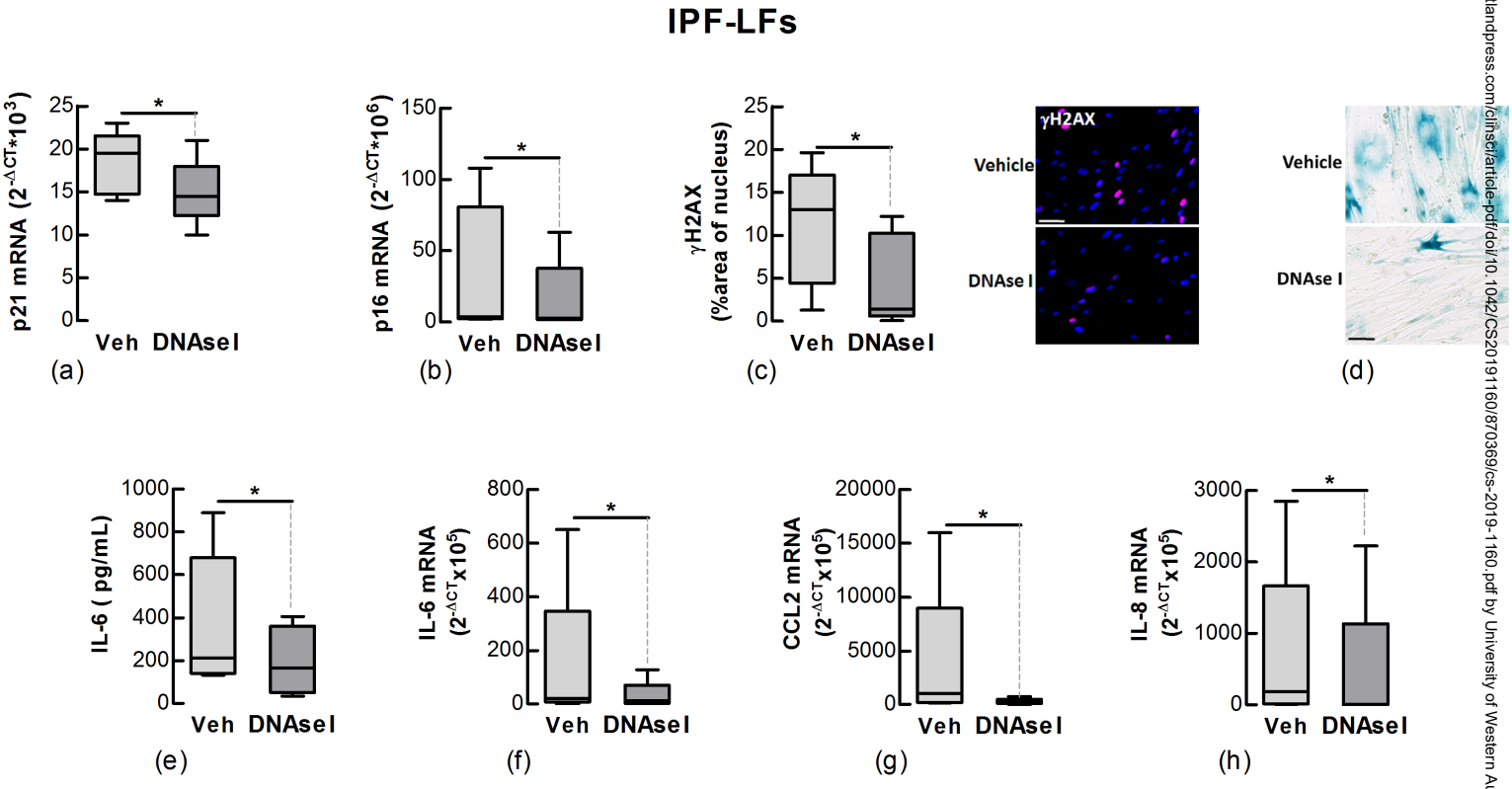

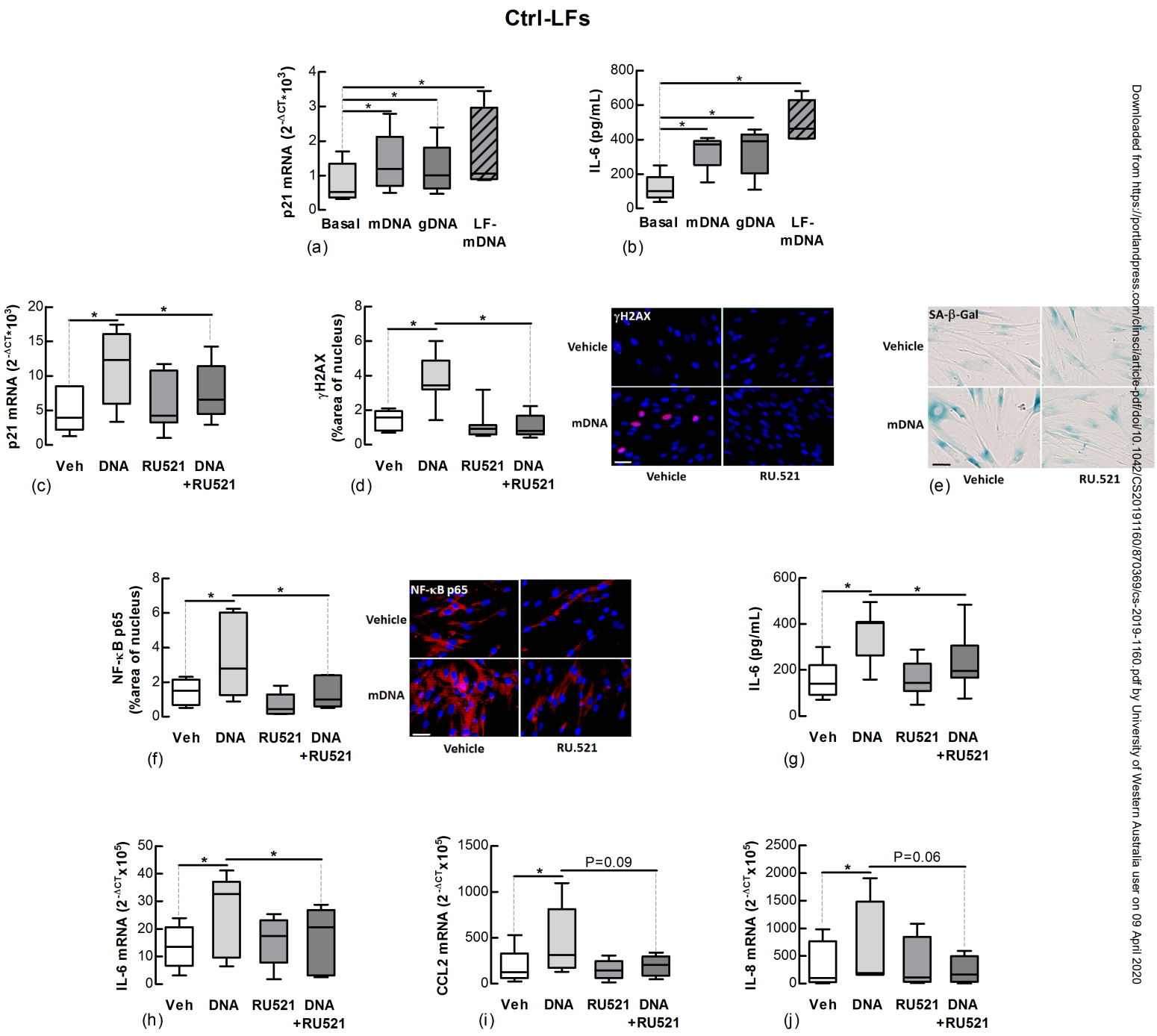

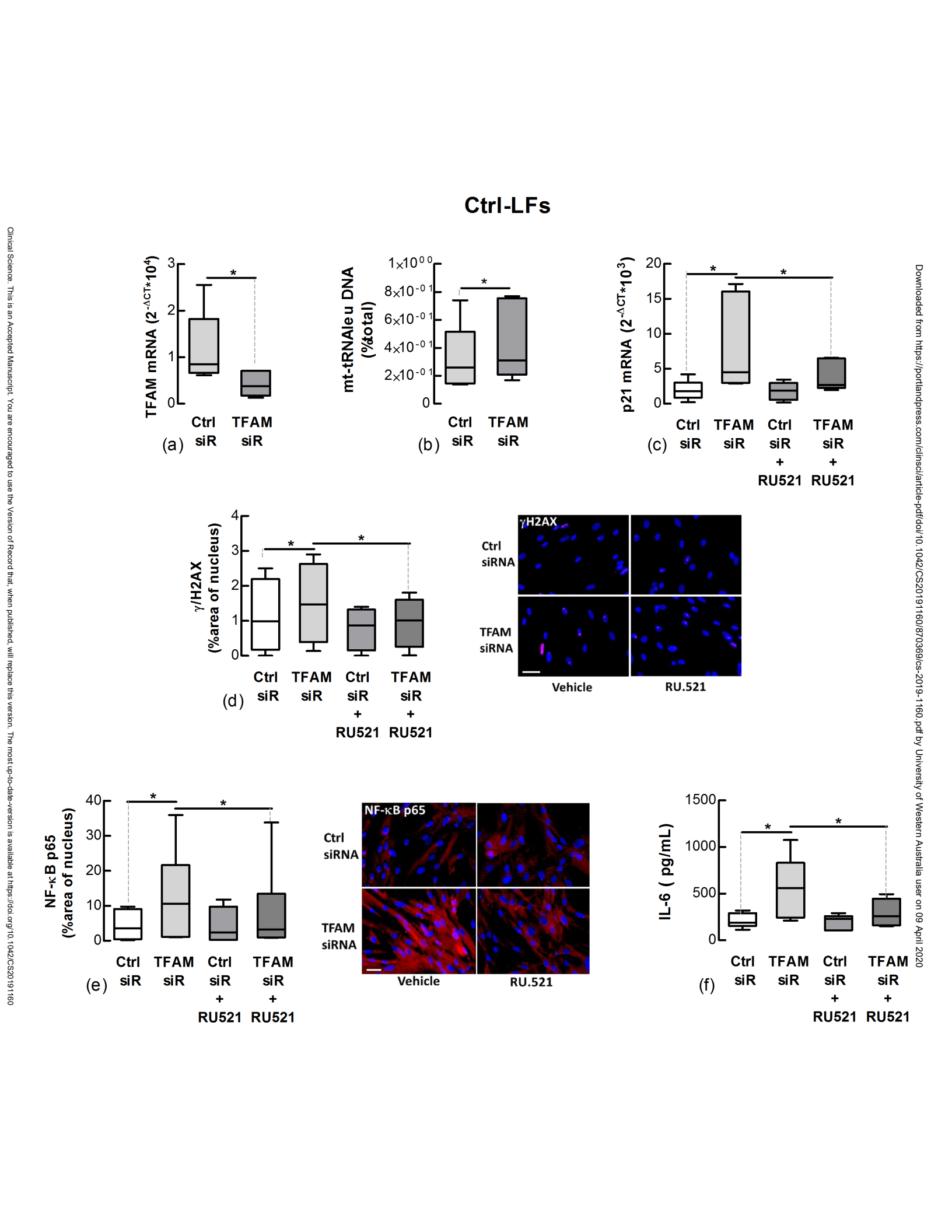

Ctrl-LFs

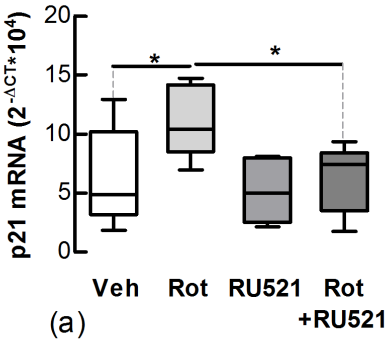

(a)

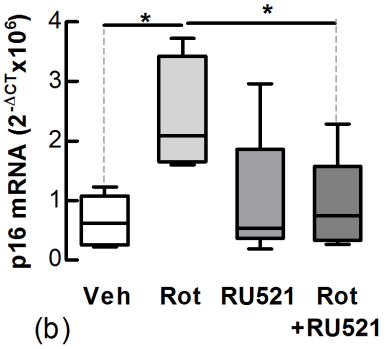

(b)

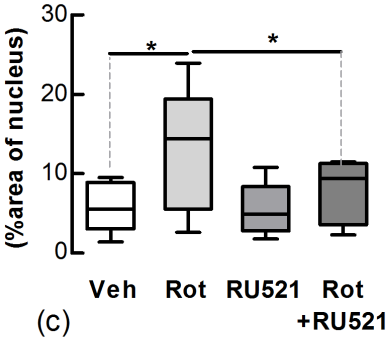

(c)

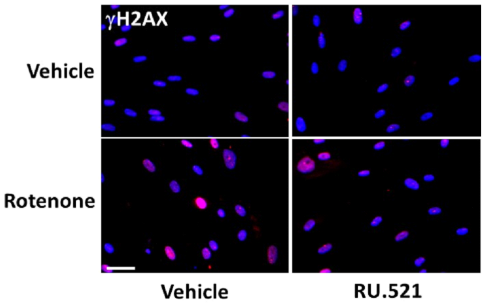

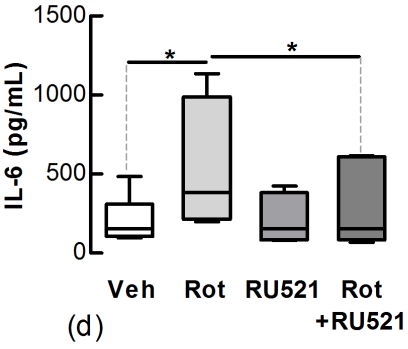

(d)

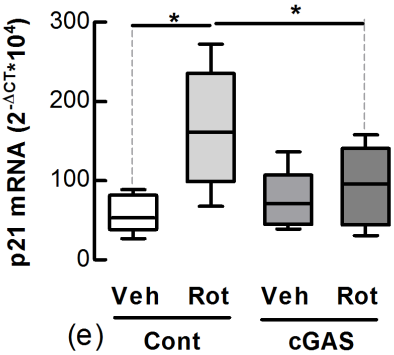

(e)

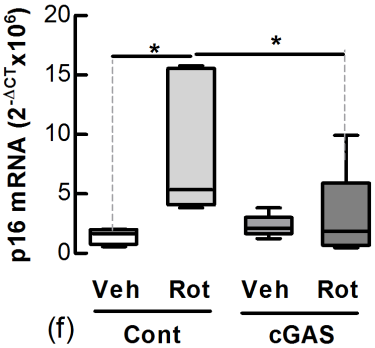

(f)

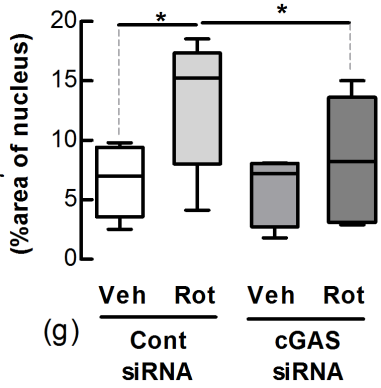

(g)

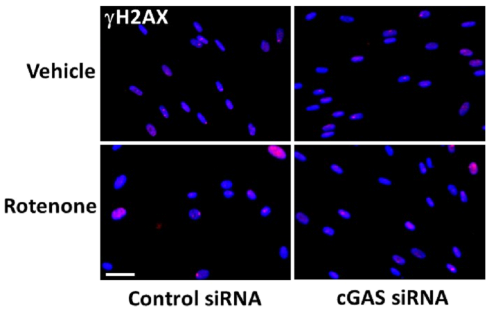

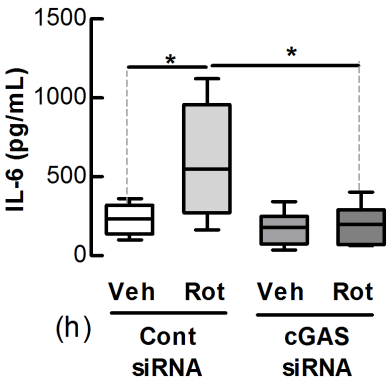

(h)